2010 IEEE International Conference on Robotics and Automation
Anchorage Convention District
May 3-8, 2010, Anchorage, Alaska, USA

Analytical Modeling and Experimental Studies of Robotic Fish Turning

Xiaobo Tan, Michael Carpenter, John Thon and Freddie Alequin-Ramos

Abstract— **Turning is one of the most important maneuvers for biological and robotic fish. In our group's prior work, an analytical framework was proposed for modeling the steady turning of fish, given asymmetric, periodic body/tail movement or deformation. However, the approach was not illustrated with simulation or validated with experiments. The contributions of the current paper are three fold. First, an extension to the modeling framework is made with a more rigorous formulation of the force balance equation. Second, we have worked out two examples explicitly, one with an oscillating, rigid tail, and the other with a flexible tail having a uniform curvature, and compared their turning behaviors through numerical results. Third, for model validation purposes, a robotic fish prototype has been developed, with the tail shaft controlled precisely by a servo motor. For a rigid tail, experimental results have confirmed the model prediction that, for the tested range, the steady-state turning radius and turning period decrease with an increasing bias in the tail motion, and that the turning period drops with an increasing tail beat frequency. We have also found that, with a flexible fin attached to the tail shaft, the robot can achieve faster turning with a smaller radius than the case of a rigid fin, and modeling within the same framework is underway to understand this phenomenon.**

I. Introduction

There is a tremendous interest in developing highly maneuverable and efficient robotic fish [1]–[10]. In contrast to underwater vehicles powered by propellers, these robots achieve locomotion and maneuvering through deformation and movement of the body and fin-like devices which are often actuated with motors [9], [11], [12] or smart materials [3], [7], [8], [13], [14]. An important maneuver for robotic fish, as is for biological fish, is the turning. Turning has been studied extensively in experimental and mathematical biology. For example, wake dynamics and fluid forces during the turning maneuver of a sunfish were studied by Drucker and Lauder [15], and the kinematics and muscle dynamics of carp in sharp turn during C-start were examined by Spierts and van Leeuwen [16]. Weihs performed hydrodynamic analysis of turning maneuvers of real fish using the slender body theory [17]. In robotics, turning strategies for robotic fish have been studied analytically and experimentally [18]–[20].

This work was supported in part by ONR (grant N000140810640, program manager Dr. T. McKenna) and NSF (ECCS 0547131, CCF 0820220, CNS 0751155, IIS 0916720).

X. Tan, M. Carpenter, J. Thon, and F. Alequin-Ramos are with the Smart Microsystems Laboratory, Department of Electrical and Computer Engineering, Michigan State University, East Lansing, MI 48824, USA. J. Thon is also with Holt Public Schools, 1784 Aurelius Rd, Holt, MI 48842. xbtan@egr.msu.edu (X. T.), carpe216@msu.edu (M. C.), jthon@hpsk12.net (J. T.), freddie.alequin@gmail.com (F. A.)

Send correspondence to X. Tan. Tel: 517-432-5671; Fax: 517-353-1980.

It is desirable to have an *analytical* understanding of turning behavior in terms of the body and/or fin movement, which would be instrumental in the design and control of robotic fish. Existing modeling work extracts turning information from simulated trajectories based on dynamics-governing equations (e.g., [19], [20]), which is time-consuming and does not provide much direct insight. In our group's prior work [21], a modeling framework was proposed for the computation of steady-state turning motion given asymmetric, periodic body/tail deformation of a robotic fish. In this approach it is postulated that the two key parameters of turning motion, the radius and the period, can be obtained by solving the implicit force and moment balance equations for the averaged, steady-state motion, where the hydrodynamic force and the resulting moment are evaluated with Lighthill's large-amplitude elongated-body theory [22]. However, the modeling framework was not illustrated with simulation results or validated in experiments.

The contributions of the current paper lie in the extension, illustration, and experimental validation of the analytical modeling framework originally proposed in [21]. First, we provide a modified, more rigorous formulation for the force balance equation, which is consistent with the classical case of forward swimming [23]. Second, two examples are worked out explicitly to illustrate the modeling approach. The first example is a robotic fish with a rigid tail that oscillates periodically with a fixed bias angle, while the second example deals with a flexible tail having a uniform curvature, where the curvature varies periodically with a fixed bias. In both cases, explicit equations of the turning radius and turning period (or angular frequency of turning) are derived in terms of the tail gait parameters. Numerical results are provided to illustrate the turning behavioral differences between the two tails.

For model validation purposes, we have further developed a robotic fish prototype, with the tail shaft controlled precisely by a servo motor. Different passive fins can be attached to the shaft. For a rigid tail, experimental data on turning have confirmed the model prediction that, for the tested range, the steady turning radius and turning period decrease when the bias in the tail motion increases, and that the turning period drops when the tail beat frequency increases. A flexible passive fin has also been amounted on the tail shaft, and with the same input to the servo motor, the flexible tail results in faster turning with a smaller radius than the case of a rigid tail. A closer look reveals that the flexible tail undergoes biased rotation of its base point and (approximately) symmetric change of curvature caused by the fin-fluid interactions. Work is underway to apply the

analytical modeling framework to elucidate the observed turning behavior for the flexible tail.

The remainder of the paper is organized as follows. The analytical modeling framework is described in Section II. Illustrative examples for a rigid tail and a flexible tail with uniform curvature are presented in Section III. Experimental results on a robotic fish prototype are provided in Section IV. Concluding remarks are provided in Section V.

II. The Modeling Framework for Steady Turning

A. Evaluation of the Hydrodynamic Force

The framework uses Lighthill's large-amplitude elongated-body theory [22] to evaluate the hydrodynamic reactive force experienced by a robotic fish. A frame of reference is chosen such that the water far from the fish is at rest. As illustrated in Fig. 1, the $x-$ and $z-$axes are horizontal while the $y-$axis is vertical (pointing into water). The fluid is considered to be inviscid. It is assumed that the fish swims at a fixed depth $y=0$ and thus moves only in the horizontal $x-z$ plane. The spinal column of the fish is assumed to be inextensible and is parameterized by a, with $a=0$ denoting the anterior end of the fish and $a=L$ denoting the posterior end. The coordinates $(x(a,t),z(a,t)), 0\le a\le L$, denotes the time trajectory of each point a on the spinal column, which could be due to fish body/fin undulation or the resulting translational/rotational motion of the whole fish.

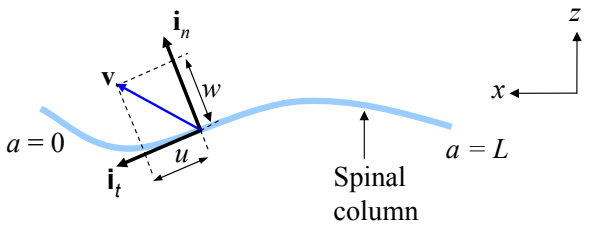

Fig. 1. Illustration of the coordinate system for the spinal column of fish (view from top).

Following Lighthill [22], given $(x(a,t),z(a,t))$, the hydrodynamic reactive force density at each point $a<L$ is

$$\mathbf{f}(a)=\begin{pmatrix} f_x(a)\\ f_z(a)\end{pmatrix}=-m\frac{d}{dt}(w\mathbf{i}_n), \tag{1}$$

and at $a=L$, there is a concentrated force

$$\mathbf{F}_L=\begin{pmatrix} F_{Lx}\\ F_{Lz}\end{pmatrix}=\left[\frac{1}{2}mw^2\mathbf{i}_t-umw\mathbf{i}_n\right]_{a=L}. \tag{2}$$

In (1) and (2), m denotes the virtual mass per unit length and can be approximated by $\frac{1}{4}\pi\rho s^2$, where ρ is the density of water and s is the depth of the cross-section. As illustrated in Fig. 1, $\mathbf{i}_t=(-\partial x/\partial a,-\partial z/\partial a)^T$ and $\mathbf{i}_n=(\partial z/\partial a,-\partial x/\partial a)^T$ (with ^{T} denoting transpose) represent the unit vectors tangential and perpendicular to the spinal column, respectively, and u and w represent the components of the velocity $\mathbf{v}=(\partial x/\partial t,\partial z/\partial t)^T$ at a in $\mathbf{i}_t$ and $\mathbf{i}_n$ directions, respectively:

$$u = <\mathbf{v},\mathbf{i}_t>=-\frac{\partial x}{\partial t}\frac{\partial x}{\partial a}-\frac{\partial z}{\partial t}\frac{\partial z}{\partial a}, \tag{3}$$

$$w = <\mathbf{v},\mathbf{i}_n>=\frac{\partial x}{\partial t}\frac{\partial z}{\partial a}-\frac{\partial z}{\partial t}\frac{\partial x}{\partial a}. \tag{4}$$

B. Analytical Modeling of Steady Turning

While the theory in Section II-A allows one to evaluate the reactive force *given* the motion trajectories $(x(a,t),z(a,t))$, it cannot predict the motion given the body/tail deformation. If we view the motion of a fish or robotic fish as the sum of the global, rigid-body motion (translation and rotation) and the local deformation or movement of body/fin, it is desirable to understand what would be the global motion given the local movement. This problem is of particular interest for robotic fish, because the local movement is typically generated through actuation (an input that can be manipulated) and the global motion represents the outcome.

We consider the steady turning motion of a robotic fish under general, periodic, asymmetric movement of body and/or fin. For ease of presentation, however, we will focus on the case of a carangiform robotic fish, consisting of a rigid body part and a caudal fin. It is expected that, under periodic, asymmetric tail movement, the robotic fish will settle down to a "steady" turning motion[1]. The key parameters of interest are the turning radius R and the turning period T_1 (or equivalently, the angular velocity of turning, $\omega_1=2\pi/T_1$). By taking R and ω_1 as unknowns, one can first derive $(x(a,t),z(a,t))$ in terms of the global motion characterized by R and ω_1 and the given tail motion. Hydrodynamic reactive force and the resulting moment can be evaluated using (1) and (2). Force and moment balance equations will then lead to implicit equations involving R and ω_1, the solution of which provides the values of R and ω_1. A more detailed account of the approach follows.

Fig. 2 shows the coordinate systems used. The $x-z$ coordinate system is the global reference system and does not change with time. On the other hand, there is a moving coordinate system $x'-z'$ attached to the body of the robotic fish, with $z'-$axis pointing to the heading direction of the robot. The periodic tail movement relative to the body is specified by $(x'(a,t),z'(a,t))$ with some period T_0. The origin of the moving frame is set to be at the center O' of inertia of the robot. For ease of discussion, we assume that the center of mass is also located at O'. The distance between O' and the beginning of tail ($a=0$) is denoted as c. As mentioned earlier, the robot is assumed to swim on the circle with radius R, at an angular velocity of ω_1. Consequently, the $x'-$axis coincides with the ray connecting the origin of $x-z$ frame to the center of the robot.

Without loss of generality, we take the angle α between the $x-$ and $x'-$axes to be $\omega_1 t$. The trajectory of a in the

[1]Strictly speaking, the hydrodynamics is constantly under an unsteady state. By "steady" turning, we mean that the mean motion averaged over the actuation period is constant.

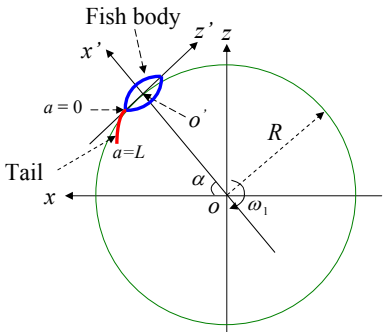

Fig. 2. The inertial $x-z$ frame and the moving $x'-z'$ frame on the robotic fish, which swims in a circle.

$x-z$ frame can then be represented by

$$\begin{pmatrix} x(a,t) \\ z(a,t) \end{pmatrix} = \begin{pmatrix} x_{o'}(t) \\ z_{o'}(t) \end{pmatrix} + \begin{bmatrix} \cos\alpha & -\sin\alpha \\ \sin\alpha & \cos\alpha \end{bmatrix} \begin{pmatrix} x'(a,t) \\ z'(a,t) \end{pmatrix}, \quad (5)$$

where $\alpha = \omega_1 t$, and $(x_{o'}(t), z_{o'}(t))$ represents the position of center of robotic fish: $x_{o'}(t) = R\cos(\omega_1 t)$, $z_{o'}(t) = R\sin(\omega_1 t)$. The hydrodynamic force density $\mathbf{f}(a) = (f_x(a), f_z(a))^T$ and the concentrated force $\mathbf{F}_L = (F_{Lx}, F_{Lz})^T$ at $z = L$ can then be evaluated with (1) and (2), with a total force given by

$$\mathbf{F} = \begin{pmatrix} F_x \\ F_z \end{pmatrix} = \left[\frac{1}{2}mw^2\mathbf{i}_t - umw\mathbf{i}_n\right]_{a=L} - \frac{d}{dt}\int_0^L mw\mathbf{i}_n da. \quad (6)$$

Let $\mathbf{f}'(a) = (f_{x'}(a), f_{z'}(a))^T$ and $\mathbf{F}'_L = (F_{Lx'}, F_{Lz'})^T$ be the representations of $\mathbf{f}(a)$ and $\mathbf{F}_L$ in the $x'-z'$ frame, respectively. Note that

$$\mathbf{f}'(a) = \begin{pmatrix} f_{x'}(a) \\ f_{z'}(a) \end{pmatrix} = \begin{bmatrix} \cos\alpha & \sin\alpha \\ -\sin\alpha & \cos\alpha \end{bmatrix} \begin{pmatrix} f_x(a) \\ f_z(a) \end{pmatrix}, \quad (7)$$

and

$$\mathbf{F}'_L = \begin{pmatrix} F_{Lx'} \\ F_{Lz'} \end{pmatrix} = \begin{bmatrix} \cos\alpha & \sin\alpha \\ -\sin\alpha & \cos\alpha \end{bmatrix} \begin{pmatrix} F_{Lx} \\ F_{Lz} \end{pmatrix}. \quad (8)$$

The reactive force $\mathbf{F} = (F_x, F_z)^T$ in the $x-z$ frame, as a whole, can be represented in the $x'-z'$ frame as $\mathbf{F}' = (F'_x, F'_z)^T$ via transformation

$$\mathbf{F}' = \begin{pmatrix} F_{x'} \\ F_{z'} \end{pmatrix} = \begin{bmatrix} \cos\alpha & \sin\alpha \\ -\sin\alpha & \cos\alpha \end{bmatrix} \begin{pmatrix} F_x \\ F_z \end{pmatrix}. \quad (9)$$

Note that all the force terms will be functions of R, ω_1, and the tail movement pattern.

At steady turning, the robot achieves a constant tangential speed. This implies that the average of F'_z over one tail movement period T_0 will be balanced by the mean drag force in the opposite direction. Define

$$\overline{F}_t = \frac{1}{T_0}\int_0^{T_0} F'_z(t)dt. \quad (10)$$

$\overline{F}_t$ will be written as $\overline{F}_t(R,\omega_1)$ since it is a function of R and ω_1. It then follows that

$$\overline{F}_t(R,\omega_1) = \frac{C_d\rho S(\omega_1 R)^2}{2}, \quad (11)$$

where C_d is the drag coefficient, and S is the wetted surface area. Note that in our group's prior work [21], the mean centripetal force was involved in the force balance equation. Comparing to the earlier approach, Eq. (11) is a more rigorous formulation and effectively accommodates the effect of drag, and it is consistent with the approach used by Lighthill in deriving the forward swimming speed of a fish [23].

At steady turning, the robot also undergoes constant rotation and thus the moment balance equation holds. The moment τ generated by $\mathbf{f}'(a)$ and $\mathbf{F}'_L$ with respect to O' can be evaluated as

$$\tau(t) = \int_0^L f_{z'}(a)x'(a,t) - f_{x'}(a)z'(a,t)da + F_{Lz'}x'(L,t) - F_{Lx'}z'(L,t). \quad (12)$$

Define the average of τ over the period T_0 as

$$\bar{\tau} = \frac{1}{T_0}\int_0^{T_0}\tau(t)dt. \quad (13)$$

Note that $\bar{\tau}$ will be a function of R and ω_1, so we write $\bar{\tau}(R,\omega_1)$. The moment balance equation reads

$$\bar{\tau}(R,\omega_1) = \gamma\omega_1, \quad (14)$$

where γ is the rotational damping coefficient of the robot.

Eqs. (11) and (14) form a pair of equations involving the two unknowns R and ω_1. By solving these two equations jointly, we can obtain the values of turning radius R and angular velocity ω_1 for the given pattern of tail movement.

III. Illustrative Examples

In this section we illustrate the analytical modeling approach with examples. As shown in Fig. 3, two types of tail movement are considered. The first is an oscillating rigid tail, with the angle θ satisfying

$$\theta(t) = \theta_b + \theta_0\sin(\omega_0)t, \quad (15)$$

where θ_b and θ_0 denote the bias and the amplitude of the tail oscillation, respectively. In the second case (Fig. 3(b)), the tail is flexible with a uniform curvature throughout its length, and we assume that the curvature $\kappa(t)$ satisfies

$$\kappa(t) = \kappa_b + \kappa_0\sin(\omega_0)t, \quad (16)$$

where κ_b and κ_0 denote the bias and the amplitude of curvature variation. Note that an ionic polymer-metal composite (IPMC) caudal fin could produce a uniform curvature that varies according to (16) with a biased sinusoidal voltage input, if the surface resistance of the IPMC material is zero [24].

We assume that both tails have a uniform width b. For the rigid tail case, one can show that the final force and moment balance equations take the following form:

$$a_0 + a_1\omega_1 + a_2\omega_1^2 + a_3\omega_1 R + a_4\omega_1^2 R + a_5\omega_1^2 R^2 = 0, \quad (17)$$

$$A_0 + A_1\omega_1 + A_2\omega_1^2 + A_3\omega_1 R + A_4\omega_1^2 R + A_5\omega_1^2 R^2 = 0, \quad (18)$$

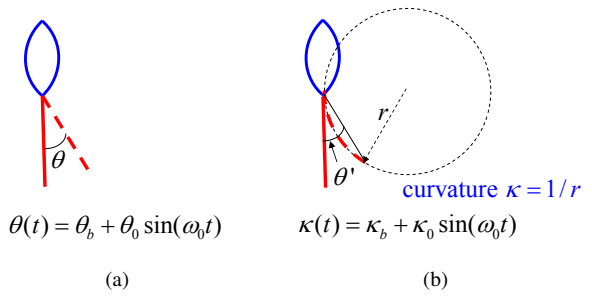

Fig. 3. Definitions of tail movement patterns. (a) Rigid tail; (b) Flexible tail with uniform curvature.

where the coefficients are evaluated as

$$
\begin{aligned}
a_0 &= -\frac{1}{T_0}\int_0^{T_0} L^2\sin(\theta)\ddot{\theta}\,dt,\\
a_1 &= \frac{1}{T_0}\int_0^{T_0} 2cL\dot{\theta}\sin^2\theta\,dt,\\
a_2 &= \frac{1}{T_0}\int_0^{T_0} \left[c^2\cos\theta(1+\sin^2\theta)+cL(1-\cos 2\theta)\right]dt,\\
a_3 &= \frac{1}{T_0}\int_0^{T_0} \left[2c\sin^3\theta-2L\dot{\theta}\sin(2\theta)\right]dt,\\
a_4 &= -\frac{1}{T_0}\int_0^{T_0} L\sin(2\theta)\,dt,\\
a_5 &= -\frac{1}{T_0}\int_0^{T_0} \left[\sin^2\theta\cos\theta+\frac{C_d\rho S}{m}\right]dt,\\
A_0 &= -\frac{1}{T_0}\int_0^{T_0} \left[cL^2\ddot{\theta}\cos\theta+\frac{2}{3}L^3\ddot{\theta}\right]dt,\\
A_1 &= \frac{1}{T_0}\int_0^{T_0} \left[3cL^2\dot{\theta}\sin\theta+2c^2L\dot{\theta}\sin(2\theta)-\frac{2\gamma}{m}\right]dt,\\
A_2 &= \frac{1}{T_0}\int_0^{T_0} \left[2c^2L\sin(2\theta)+2cL^2\sin\theta\right.\\
&\quad \left.+c^3\sin(2\theta)\cos\theta-c^3\sin\theta\cos^2\theta\right]dt,\\
A_3 &= -\frac{1}{T_0}\int_0^{T_0} \left[3L^2\dot{\theta}\cos\theta+4cL\dot{\theta}\cos^2\theta\right]dt,\\
A_4 &= -\frac{1}{T_0}\int_0^{T_0} \left[cL+2L^2\cos\theta+3cL\cos(2\theta)\right.\\
&\quad \left.+2c^2\cos^3\theta\right]dt,\\
A_5 &= -\frac{1}{T_0}\int_0^{T_0} \left[(L+c\cos\theta)\sin(2\theta)-c\sin^3\theta\right]dt,
\end{aligned}
$$

where $T_0 = 2\pi/\omega_0$, and θ denotes the time function $\theta(t)$.

For the flexible tail with a uniform curvature function $\kappa(t)$, it can be shown that the force and moment balance equations take the same form as (17) and (18), but the expressions for the coefficients are much longer and thus omitted here because of space limitation.

Fig. 4 and Fig. 5 show the numerical results for the two cases. The parameters used in the computation are: $L = 0.08$ m, $b = 0.015$ m, $c = 0.07$ m, $C_d = 0.01$, $\rho = 1000\ \mathrm{kg/m^3}$, $S = 0.01\ \mathrm{m^2}$, and $\gamma = 2.5\times10^{-4}$. Eqs. (17) and (18) are solved using the *fsolve* command in Matlab. For both cases, it can be seen that, when the bias increases, the turning radius becomes smaller, which is consistent with one's intuition. The effect of bias on the turning period is more interesting, since it seems that, for both cases, there exists an optimal bias that minimizes the turning period. In the simulation, we have made the two tail movements somewhat comparable in the following sense: the angle θ' defined in Fig. 3(b) for the curvature case is equal to θ defined in Fig. 3(a) for the rigid tail case. From the numerical results in Figs. 4 and 5, it appears that for "comparable" tail movement, the curvature-controlled tail results in a smaller turning radius and smaller turning period than the bending-controlled tail. To some extent, this difference also indicates the advantage of a flexible tail in maneuvering.

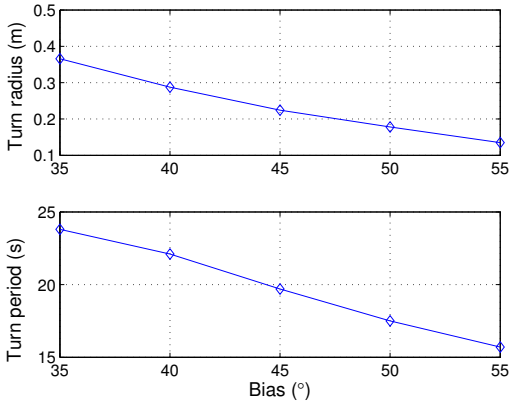

Fig. 4. Simulation results for a rigid fin: turning radius and period versus bias angle. In all cases, the tail beats at 1 Hz with amplitude 10°.

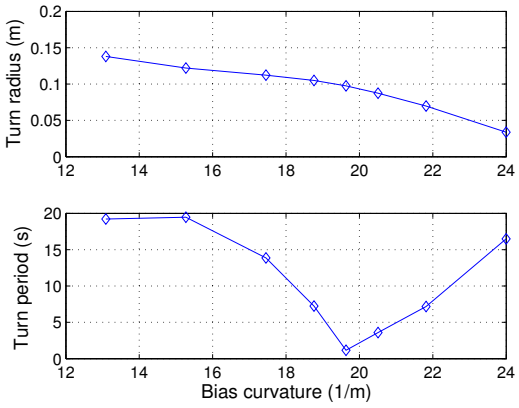

Fig. 5. Simulation results for a flexible fin with uniform curvature: turning radius and period versus bias curvature. In all cases, the tail deforms at 1 Hz with curvature amplitude $4.36\,\mathrm{m^{-1}}$.

IV. Experimental Results

A robotic fish prototype has been constructed to further validate the modeling approach. As shown in Fig. 6, a servo motor (HS-5085MG from Hitec) is used to control the angular position of a tail shaft through a chain transmission mechanism. A slit is cut in the shaft, where a tail can been inserted and secured with screws. The shell of the robot

is custom-made with fiberglass and carbon fiber. Control signals and power to the servo motor are provided through thin, flexible wires (Ultra-Flex Miniature Wire 36 Awg from McMaster-Carr) off the robot. A carbon fiber foil, 5.3 cm long and 1.7 cm wide, is attached to the tail shaft as a caudal fin. The foil has little deformation when moved through water and is considered to be rigid in this study. With a given pattern $\theta(t)$, (15), for the tail shaft, it is observed that the robot trajectory converges to a circular orbit (Fig. 7). Videos of the robot motion are taken and processed to extract the turning radius and period for a given tail pattern.

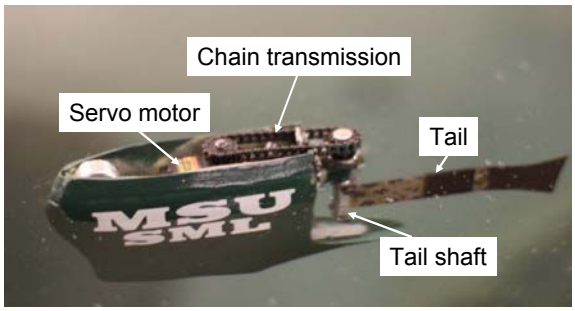

Fig. 6. A robotic fish prototype with a servo-driven tail.

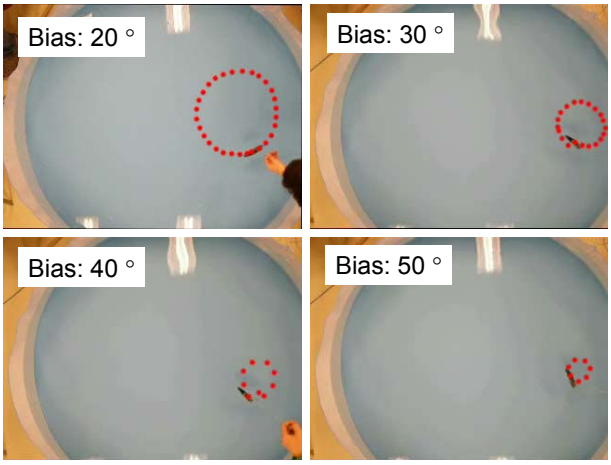

Fig. 7. Turning trajectories of the robotic fish with different bias angles. In all cases, the tail beats at 2 Hz with amplitude 22.5°.

Fig. 7 shows the circular paths of the robot when the tail beats at 2 Hz with amplitude $\theta_0 = 22.5°$ but with different bias angles. It can be seen that the turning radius decreases as the bias angle θ_b increases. Fig. 8 shows the comparison between the measured turning parameters and the model predictions. The following additional parameters for the model have been identified and used in numerical computation: $c = 0.047$ m, $S = 0.014\,\mathrm{m}^2$, $C_d = 0.13$, and $\gamma = 2.5 \times 10^{-4}$. From the figure, for the tested range, the model has predicted correctly the decreasing turning radius and period when the bias is increased, with good, quantitative agreement with the experimental data. The model has been further validated with a different set of experimental conditions. As shown in Fig. 9, the model is able to predict how the turning period changes when one varies the tail beat frequency.

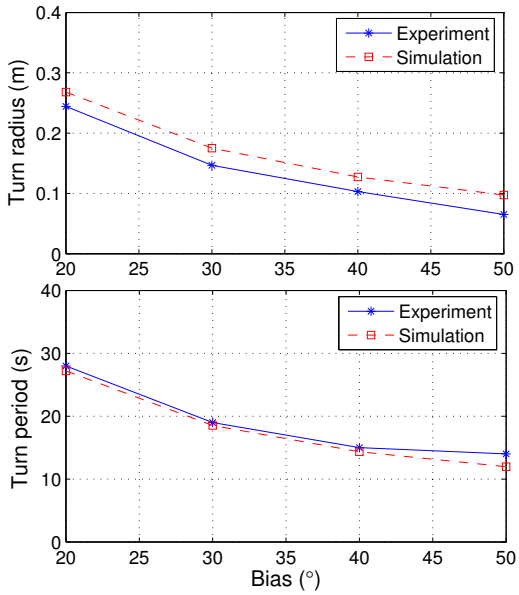

Fig. 8. Experimental validation of the turning model: turning radius and period versus bias angle. In all cases, the tail beats at 2 Hz with amplitude 22.5°.

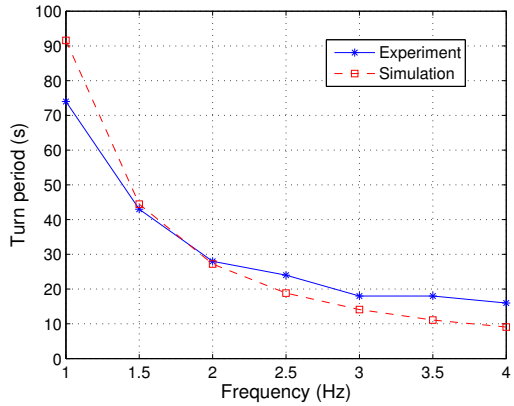

Fig. 9. Experimental validation of the turning model: turning period versus tail beat frequency. In all cases, the tail beats with bias 20° and amplitude 22.5°.

We have also conducted experiments with different tail materials to examine the effect of tail stiffness on turning. A transparency film (from 3M) is cut into the same size as that of the rigid tail and attached to the tail shaft. When moved through water by the servo motor, the film deforms, as can be seen in Fig. 10. Here the robot is anchored and the tail movement is captured by a CCD camera (Grasshopper from Point Grey Research Inc.) at 120 frames per second. The base point of the flexible tail, where the tail connects to the shaft, is highlighted. From the figure, the motion of the flexible tail is a combination of the base point translation (with the

shaft) and the tail shape change due to fin-fluid interactions. The curvature of the tail is approximately uniform along the length, and it tends to be maximum when the tail shaft reverses. Note that the flexible tail movement here is different from the one considered in Fig. 3(b) in that it has a moving base point and its curvature change does not appear to be biased. So we cannot apply the analytical results presented in Section III, but the experimental results below are of interest in their own right.

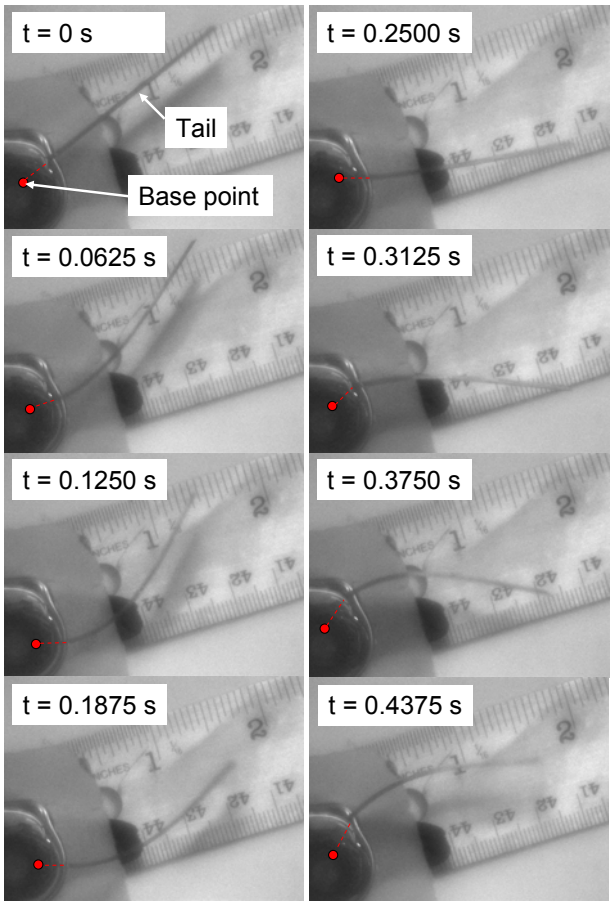

Fig. 10. Snapshots of the flexible tail beating at 2 Hz with bias 20° and amplitude 52.5°. The body of the robotic fish is anchored.

Figs. 11 and 12 compare the rigid and flexible tails on their turning performance under a wide range of tail beat conditions. It can be observed that, in general, the robot turns faster with a smaller turning radius when equipped with the flexible tail, for the same motion of the tail shaft. The only exception is that, when the tail beat frequency gets high (above 2 Hz), the period of turning with the flexible tail seems to become longer (Fig. 12). This counterintuitive phenomenon might be explained by that, due to the relatively low resonant frequency of the flexible tail, the amplitude of curvature change drops as the beat frequency increases, as shown in Fig. 13.

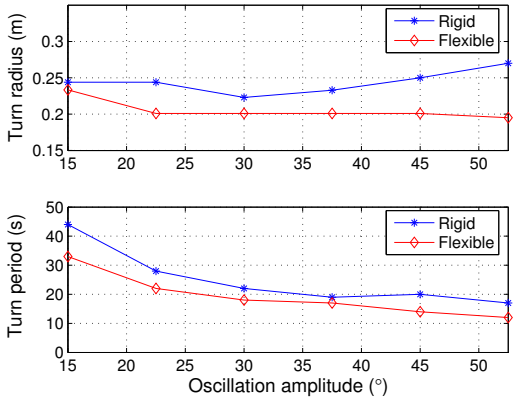

Fig. 11. Experimental comparison of turning performance between rigid and flexible tails: turning radius and period versus tail oscillation amplitude. In all cases, the tail beats at 2 Hz with bias 20°.

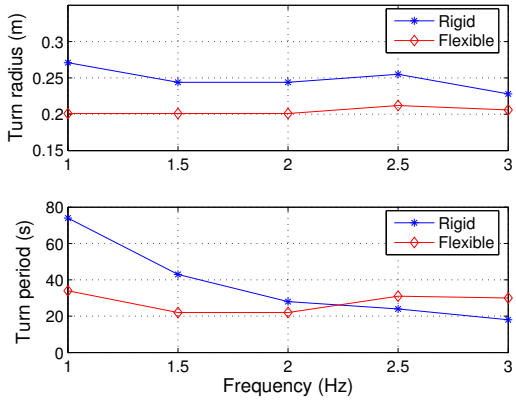

Fig. 12. Experimental comparison of turning performance between rigid and flexible tails: turning radius and period versus tail beat frequency. In all cases, the tail beats with bias 20° and amplitude 22.5°.

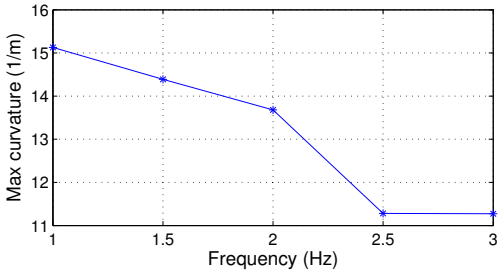

Fig. 13. Measured maximum tail curvature versus tail beat frequency for the flexible tail. In all cases, the tail beats with bias 20° and amplitude 22.5°.

V. Conclusion and Future Work

In this paper we have provided two numerical examples to illustrate an analytical approach to the modeling of steady turning of robotic fish. For an oscillating, perfectly rigid

tail, and a flexible tail with curvature control, the force and moment balance equations have been derived explicitly in terms of two unknowns, the turning period and the turning radius. Numerical results have been obtained, which provide interesting comparisons between the two cases. We have further validated the model with experiments on a robotic fish prototype, for the case of a perfectly rigid tail. When tails with different stiffness are attached to the tail shaft, we have observed that a flexible tail tends to result in faster turning with a smaller radius than a rigid tail.

Future work will be carried out in several directions. First, the force and moment balance equations, (11) and (14), are highly nonlinear and can admit multiple solutions. We will examine the properties of these equations to provide insight as to how to pick parameters (including initial values for the solutions) for the solver. Second, the robotic fish prototype used in this paper was tethered. Although the wires were flexible, they introduced difficulty and errors in characterizing the turning motion. Therefore, an untethered robot with onboard power and control will be instrumental in providing more accurate measurements. Third, we will apply the modeling framework to elucidate the observed turning phenomenon for the case of a flexible passive tail attached to the servo-driven shaft.

REFERENCES

[1] M. S. Triantafyllou and G. S. Triantafyllou, "An efficient swimming machine," *Scientific America*, vol. 273, no. 3, pp. 64–70, 1995.

[2] R. Mason, "Fluid locomotion and trajectory planning for shape-changing robots," Ph.D. dissertation, California Institute of Technology, 2003.

[3] S. Guo, T. Fukuda, and K. Asaka, "A new type of fish-like underwater microrobot," *IEEE/ASME Transactions on Mechatronics*, vol. 8, no. 1, pp. 136–141, 2003.

[4] J. H. Long, A. C. Lammert, C. A. Pell, M. Kemp, J. A. Strother, H. C. Crenshaw, and M. J. McHenry, "A navigational primitive: Biorobotic implementation of cycloptic helical klinotaxis in planar motion," *IEEE Journal of Oceanic Engineering*, vol. 29, no. 3, pp. 795–806, 2004.

[5] M. Epstein, J. E. Colgate, and M. A. MacIver, "Generating thrust with a biologically-inspired robotic ribbon fin," in *Proceedings of the 2006 IEEE/RSJ International Conference on Intelligent Robots and Systems*, Beijing, China, 2006, pp. 2412–2417.

[6] H. Hu, J. Liu, I. Dukes, and G. Francis, "Design of 3D swim patterns for autonomous robotic fish," in *Proceedings of the 2006 IEEE/RSJ International Conference on Intelligent Robots and Systems*, Beijing, China, 2006, pp. 2406–2411.

[7] B. Kim, D. Kim, J. Jung, and J. Park, "A biomimetic undulatory tadpole robot using ionic polymer-metal composite actuators," *Smart Materials and Structures*, vol. 14, pp. 1579–1585, 2005.

[8] X. Tan, D. Kim, N. Usher, D. Laboy, J. Jackson, A. Kapetanovic, J. Rapai, B. Sabadus, and X. Zhou, "An autonomous robotic fish for mobile sensing," in *Proceedings of the IEEE/RSJ International Conference on Intelligent Robots and Systems*, Beijing, China, 2006, pp. 5424–5429.

[9] K. A. Morgansen, B. I. Triplett, and D. J. Klein, "Geometric methods for modeling and control of free-swimming fin-actuated underwater vehicles," *IEEE Transactions on Robotics*, vol. 23, no. 6, pp. 1184–1199, 2007.

[10] P. V. Alvarado and K. Youcef-Toumi, "Design of machines with compliant bodies for biomimetic locomotion in liquid environments," *Journal of Dynamic Systems, Measurement, and Control*, vol. 128, pp. 3–13, 2006.

[11] M. S. Triantafyllou, D. K. P. Yue, and G. S. Triantafyllou, "Hydrodynamics of fishlike swimming," *Annu. Rev. Fluid Mech.*, vol. 32, pp. 33–53, 2000.

[12] P. R. Bandyopadhyay, "Maneuvering hydrodynamics of fish and small underwater vehicles," *Integrative and Comparative Biology*, vol. 42, pp. 102–117, 2002.

[13] Z. Chen, S. Shatara, and X. Tan, "Modeling of biomimetic robotic fish propelled by an ionic polymer-metal composite caudal fin," *IEEE/ASME Transactions on Mechatronics*, 2009, in press, DOI: 10.1109/TMECH.2009.2027812.

[14] S. McGovern, G. Alici, V. T. Truong, and G. Spinks, "Finding NEMO (Novel Electromaterial Muscle Oscillator): A polypyrrole powered robotic fish with real-time wireless speed and directional control," *Smart Material and Structures*, vol. 18, pp. 095 009:1–10, 2009.

[15] E. G. Drucker and G. V. Lauder, "Wake dynamics and fluid forces of turning maneuvers in sunfish," *Journal of Experimental Biology*, vol. 204, pp. 431–442, 2001.

[16] I. L. Y. Spierts and J. L. Van Leeuwen, "Kinematics and muscle dynamics of C- and S-starts of carp (*cyprinus carpio* l.)," *Journal of Experimental Biology*, vol. 202, pp. 393–406, 1999.

[17] D. Weihs, "A hydrodynamical analysis of fish turning manoeuvres," *Proceedings of the Royal Society of London B*, vol. 182, pp. 59–72, 1972.

[18] K. H. an DT. Takimoto and K. Tamura, "Study on turning performance of a fish robot," in *Proceedings of the First International Symposium on Aqua Bio-Mechanisms*, 2000, pp. 287–292.

[19] J. Liu and H. Hu, "Mimicry of sharp turning behaviours in a robotic fish," in *Proceedings of the 2005 IEEE International Conference on Robotics and Automation*, Barcelona, Spain, 2005, pp. 3318–3323.

[20] J. Yu, L. Liu, and L. Wang, "Dynamics and control of turning maneuver for biomimetic robotic fish," in *Proceedings of the 2006 IEEE/RSJ International Conference on Intelligent Robots and Systems*, Beijing, China, 2006, pp. 5400–5405.

[21] Q. Hu, D. R. Hedgepeth, L. Xu, and X. Tan, "A framework for modeling steady turning of robotic fish," in *Proceedings of the IEEE International Conference on Robotics and Automation*, Kobe, Japan, 2009, pp. 2669–2674.

[22] M. J. Lighthill, "Large-amplitude elongated-body theory of fish locomotion," *Proceedings of the Royal Society of London B*, vol. 179, pp. 125–138, 1971.

[23] ——, "Aquatic animal propulsion of high hydromechanical efficiency," *Journal of Fluid Mechanics*, vol. 44, pp. 265–301, 1970.

[24] Z. Chen and X. Tan, "A control-oriented and physics-based model for ionic polymer-metal composite actuators," *IEEE/ASME Transactions on Mechatronics*, vol. 13, pp. 519–529, 2008.